Journal of Power and Energy Systems

Vol. 3, No. 2, 2009

Pressure Drop in Two-Phase Swirling Flow in a Steam Separator*

Hironobu KATAOKA**, Yusuke SHINKAI** and Akio TOMIYAMA**
**Graduate School of Engineering, Kobe University,
Rokkodai 1-1, Nada, Kobe, 657-8501, Japan
E-mail: tomiyama@mech.kobe-u.ac.jp

Abstract
Pressure drop and liquid film thickness in air-water swirling flows in a one-fifth scale model of the steam separator are measured for a wide range of gas and liquid volume fluxes. Numerical simulations based on one-dimensional single-fluid and two-fluid models are also carried out to examine the feasibility of predicting the pressure drop and film thickness in swirling flows. The pressure drop in a single-phase swirling flow is about five times as large as that in a non-swirling flow due to the increase in the frictional pressure drop. The pressure gradient and liquid film thickness in a two-phase swirling annular flow at the inlet of the pick-off-ring of the separator are well evaluated by using a standard one-dimensional two-fluid model, provided that the interfacial and wall frictions in an ordinary two-phase annular flow are multiplied by appropriate constant values.

Key words: Swirling Flow, Annular Flow, Steam Separator, Two-Fluid Model

1. Introduction

Steam separators are installed in a boiling water reactor, BWR, to split a two-phase mixture into steam and water before feeding steam to dryers and turbines. The steam separator consists of a standpipe, a diffuser with a swirler, and a barrel with several pick-off-rings, POR. Stationary vanes of the swirler apply a large centrifugal force to the flow, which makes most of water rapidly migrate toward the barrel wall. A swirling annular flow with few droplets in the gas core is, therefore, formed in the barrel. The liquid film flow is separated from the annular flow by POR.

Separator performance has been examined by using small-scale models of a separator in an air-water system [1-6] and in a steam-water system [7]. Nakao et al. [1] measured pressure drops and separator performance using a half-scale separator. They also carried out numerical simulations to predict pressure drops, carry-under, and carry-over using the three-dimensional CFD software, STAR-CD. Ikeda et al. [7] conducted similar experiments using a 45%-scale separator. Numerical simulations were also carried out to develop a separator with lower pressure drops. Terasaka et al. [2] simulated a flow around swirler vanes using a 3D two-fluid model. In spite of these studies, no detailed information on a swirling annular flow in the barrel has been reported yet. In our previous study [3,4], we therefore measured flow patterns, liquid film thicknesses, ratios of the separated liquid flow rate to the total liquid flow rate, and distributions of droplet diameter in air-water swirling annular flows in a 1/5-scale model of the separator to understand characteristics of two-phase swirling flows in the separator and to establish an experimental database which is applicable to the modeling and validation of numerical methods for predicting two-phase swirling flows in the steam separator. We also investigated the effects of POR shape on separation performance [5], and the effects of swirler shape on pressure drop and separation

*Received 27 Mar., 2009 (No. 09-0131)
[DOI: 10.1299/jpes.3.382]

performance [6] by carrying out experiments using several pick-off-rings and swirlers.

Since there are few studies on pressure drops in two-phase swirling flows in separators, pressure drops in air-water swirling flows in the 1/5-scale model are measured in this study for a wide range of gas and liquid volumetric fluxes. Numerical simulations based on one-dimensional single-fluid and two-fluid models are also carried out to examine the feasibility of predicting the pressure drop and film thickness in two-phase swirling flows.

2. Experimental setup

Figure 1 shows the experimental apparatus. It consists of the upper tank, the barrel, the diffuser, the standpipe, the plenum, the gas-liquid mixing section, the water supply system and the air supply system. The barrel, diffuser and standpipe were made of transparent acrylic resin for observation and optical measurements of two-phase flows in the separator. The size was one-fifth of the actual steam separator used in BWR. Air was supplied from the oil-free compressor (Oil-free Scroll 11, Hitachi Ltd.), via the regulator (R600-20, CKD, Ltd.) and the flowmeter (FLT-N, Flowcell, Ltd.) to the mixing section. Tap water at room temperature (293 K) was supplied from the magnet pump (MD-40RX, Iwaki, Ltd.) via the flowmeter to the mixing section. The two-phase flow formed in the mixing section flowed up through the plenum of 60 mm inner diameter D_P and 300 mm long, the standpipe of D_S = 30 mm and 200 mm long, the diffuser of 33 mm long and the barrel of D_B = 40 mm and 270 mm long.

The swirler shown in **Fig. 2**, which was made of ABS (Acrylonitrile Butadiene Styrene) resin, was installed in the diffuser to form a swirling flow in the barrel. Its shape was based on an actual swirler, which consists of eight vanes and one hub for fixing the vanes. Experiments without the swirler were also conducted to examine its effects on pressure drop.

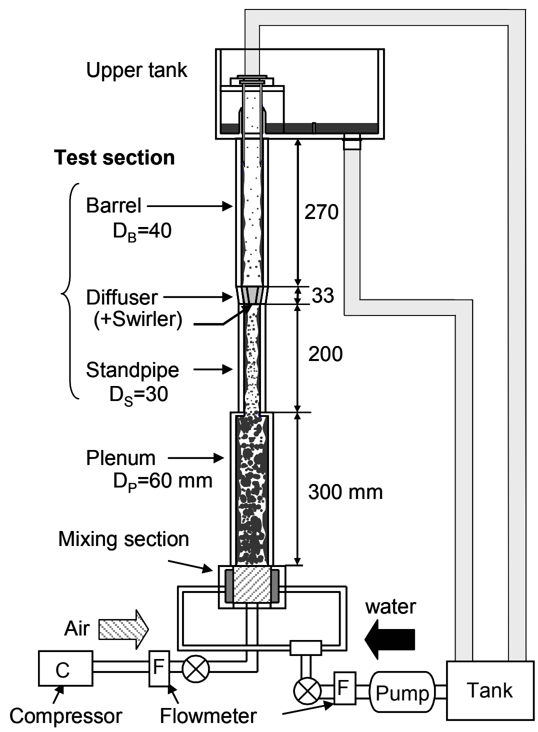

Fig. 1 Experimental apparatus

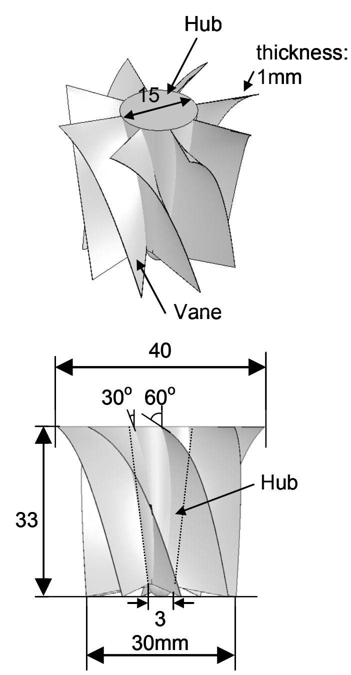

Fig. 2 Swirler shape

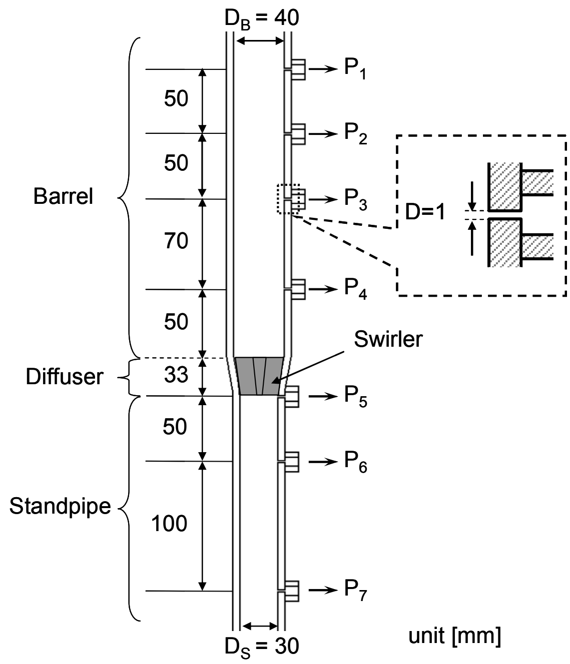

Fig. 3 Test section for measuring pressure drop

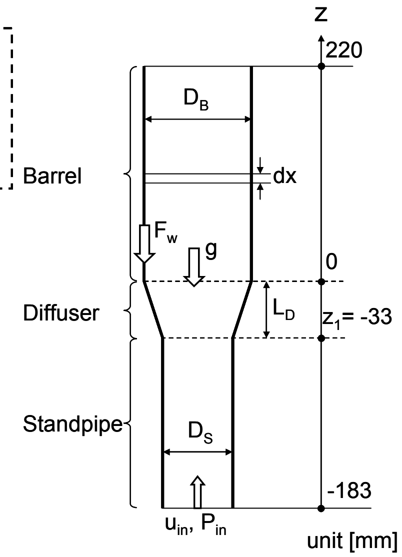

Fig. 5 Simulated region

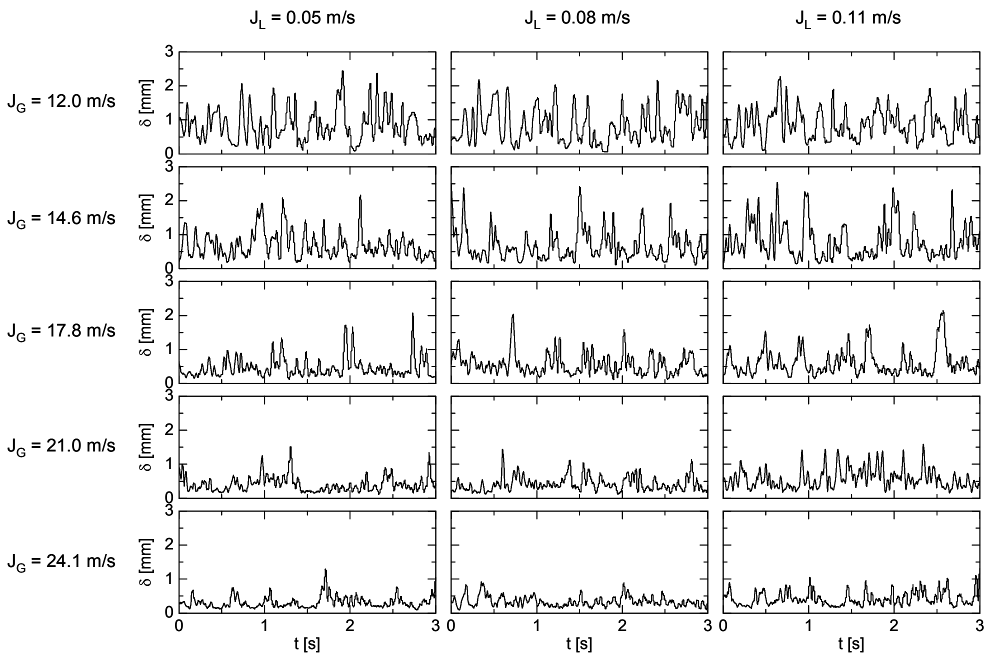

Fig. 4 Effect of J_G and J_L on δ (t)

Kataoka et al. [4] confirmed that steam-water annular swirling flow in a separator can be simulated with air-water flow if we adjust the gas and liquid volume fluxes so as to make the flow quality and the two-phase centrifugal force in the two systems the same as Nakao et al. [1] had done. Experimental conditions were, therefore, determined by adjusting the values of the flow quality and the two-phase centrifugal force to cover those in the nominal operating condition of the separator for the uprated BWR. The values of the flow quality x, the gas and liquid volume fluxes in the barrel, J_G and J_L, corresponding to the nominal operating condition were 0.18, 14.6 m/s, and 0.08 m/s, respectively [5]. Hence the present experiments were carried out for a wide range of volume fluxes including the nominal condition, i.e., J_G = 8.0 – 24.1 m/s and J_L = 0.05 – 0.11 m/s, to cover possible operating conditions of the uprated BWR.

Pressure drops in the test section were measured using differential pressure transducers (DP45, Valydine, Ltd.). As shown in **Fig. 3**, seven pressure tappings with a hole of 1 mm diameter were installed along the test section. The sampling period of the pressure measurement was 1.0 ms and the measurement time was 50 seconds, which was long enough to obtain accurate time-averaged pressures. The uncertainty estimated at 95% confidence in measured pressures was 0.3%.

The film thickness δ was measured using a laser focus displacement meter (LFD, LT-9030, Keyence, Ltd.) [8] at 170 mm above the swirler. Note that this location corresponds to the location of the inlet of the first POR in the actual steam separator. Hence we measured δ at the inlet of the first POR of the separator. The sampling period was 0.64 ms and the measurement time was 32 seconds. Hence the sampling number was 50000 points, which were large enough to obtain an accurate time-averaged film thickness δ_{mean}. Some examples of time-series data of liquid film thickness δ are shown in **Fig. 4**. The fluctuation of δ decreases as J_G increases. This is due to the increase in the centrifugal force, i.e., larger centrifugal force makes the liquid film interface smoother. The uncertainty in measured δ was 0.65 %.

3. Models for numerical simulation

3.1. Single-fluid model

The geometry of the simulated region is shown in **Fig. 5**. The following mass and momentum equations are used to compute pressure distributions in a gas single-phase flow and in a liquid single-phase flow:

$$\frac{\partial uA}{\partial z} = 0 \tag{1}$$

$$\rho \frac{\partial u^2 A}{\partial z} = -A\frac{\partial P}{\partial z} - \rho g A - F_w \tag{2}$$

where z is the axial coordinate, u the velocity, P the pressure, A the cross-sectional area, ρ the density, g the acceleration of gravity and F_w the wall friction. The wall friction is given by

$$F_w = \frac{1}{2} f_w \rho u^2 Pe \tag{3}$$

where f_w is the friction factor and Pe the wetted perimeter. The friction factor is given by

$$f_w = 0.079 Re^{-1/4} \qquad (Re \le 1\text{x}10^5) \tag{4}$$

$$f_w = 8\text{x}10^{-4} + 0.05525 Re^{-0.237} \qquad (Re > 1\text{x}10^5) \tag{5}$$

Here Re is the Reynolds number defined by $Re = \rho u D/\mu$, where μ is the viscosity.

The perimeter in the barrel and the standpipe are constant, whereas Pe in the diffuser ($-33 \le z \le 0$ mm) is given by

$$Pe = \begin{cases} \pi D_D(z) & \text{(without swirler)} \\ \pi\sqrt{D_D(z)^2 - D_S{}^2} + \dfrac{A_{vane}}{L_D} & \text{(with swirler)} \end{cases} \tag{6}$$

where L_D is the length of the diffuser, A_{vane} the surface area of swirler vanes and $D_D(z)$ is the diameter of the diffuser at z, which is given by $D_D(z) = D_S + (D_B - D_S)(z - z_1)/L_D$ where $z_1 = -33$ mm.

The cell size Δz is 0.1 mm and the number of cells is 4030. The pressure measured at the tapping, P_7, is used for the pressure P_{in} at the inlet shown in Fig. 4.

3.2. Two-fluid model for annular flow in a vertical pipe

In our previous study [(5)], we confirmed that (1) the separation performance strongly depends on the film thickness at the inlet of POR, and (2) most of droplets deposit on the liquid film before reaching the first POR due to the large centrifugal force of swirling flow when J_G in the barrel is larger than 8.0 m/s. We can, therefore, neglect the presence of droplets at a location close to the first POR and utilize a standard two-fluid model for predicting the film thickness and pressure gradient in the vicinity of POR.

The volumetric fraction α satisfies

$$\alpha_G + \alpha_L = 1 \tag{7}$$

where the subscripts G and L denote the gas and liquid phases, respectively. Assuming that both phases are incompressible viscous fluids, the mass equation for the phase k ($k = G$ or L) simplifies to

$$\frac{\partial \alpha_k}{\partial t} + \frac{\partial \alpha_k u_k}{\partial z} = 0 \tag{8}$$

The momentum equations for the gas and liquid phases are given by

$$\alpha_G \rho_G \left(\frac{\partial u_G}{\partial t} + u_G \frac{\partial u_G}{\partial z} \right) = -\alpha_G \frac{\partial P}{\partial z} - F_i - \alpha_G \rho_G g \tag{9}$$

$$\alpha_L \rho_L \left(\frac{\partial u_L}{\partial t} + u_L \frac{\partial u_L}{\partial z} \right) = -\alpha_L \frac{\partial P}{\partial z} + F_i - F_w - \alpha_L \rho_L g \tag{10}$$

where t is the time, and F_i the interfacial friction. The interfacial friction F_i and the wall friction F_w in Eqs. (9) and (10) are given by

$$F_i = \frac{Pe_i}{A} \frac{1}{2} f_i \rho_G u_r{}^2 = \frac{Pe_i}{A} \tau_i \tag{11}$$

$$F_w = \frac{Pe_w}{A} \frac{1}{2} f_w \rho_L u_L{}^2 = \frac{Pe_w}{A} \tau_w \tag{12}$$

where Pe_i is the perimeter of gas-liquid interface, Pe_w the wetted perimeter, f_i the interfacial friction factor, u_r the relative velocity ($u_G - u_L$), τ_i the interfacial shear stress and τ_w the wall shear stress. The perimeters are given by

$$Pe_i = \pi(D_B - 2\delta) \tag{13}$$

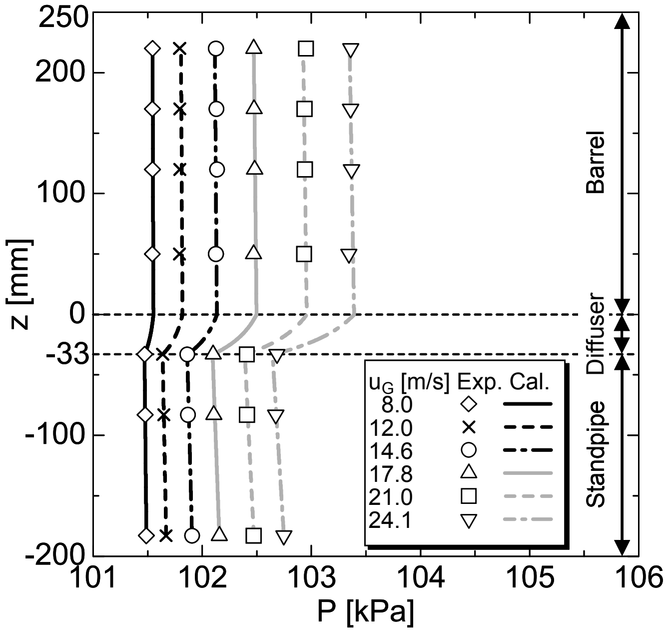

(a) Gas single-phase flow

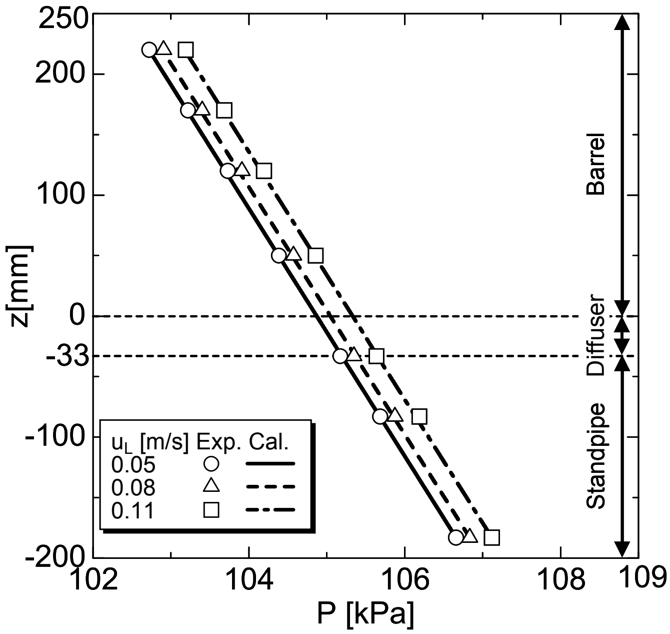

(b) Liquid single-phase flow

Fig. 6 Axial pressure distribution in non-swirling flow

$$Pe_w = \pi D_B \tag{14}$$

The friction factor f_i in Eq.(11) is calculated by using the Wallis' correlation [9]:

$$f_i = 0.079 Re_G^{-1/4} \left(1 + 300 \frac{\delta}{D_B} \right) \tag{15}$$

where Re_G is the gas Reynolds number defined by $Re_G = \rho_G J_G D_B / \mu_G$. The film thickness δ in Eqs. (13) and (15) is given by

$$\delta = D_B(1-\sqrt{\alpha_G})/2 \tag{16}$$

As in the 1D single-fluid model, f_w in Eq.(12) is calculated by

$$f_w = 0.079Re_L^{-1/4} \qquad (Re_L \le 1\text{x}10^5) \tag{17}$$

$$f_w = 8\text{x}10^{-4} + 0.05525Re_L^{-0.237} \qquad (Re_L > 1\text{x}10^5) \tag{18}$$

where Re_L is the liquid Reynolds number defined by $Re_L = \rho_L u_L D/\mu_L$.

The cell size Δz and the number of cells are 1.0 mm and 220. The pressure measured at P_4 is used for the pressure at the inlet. The initial value of film thickness is 0.2 mm.

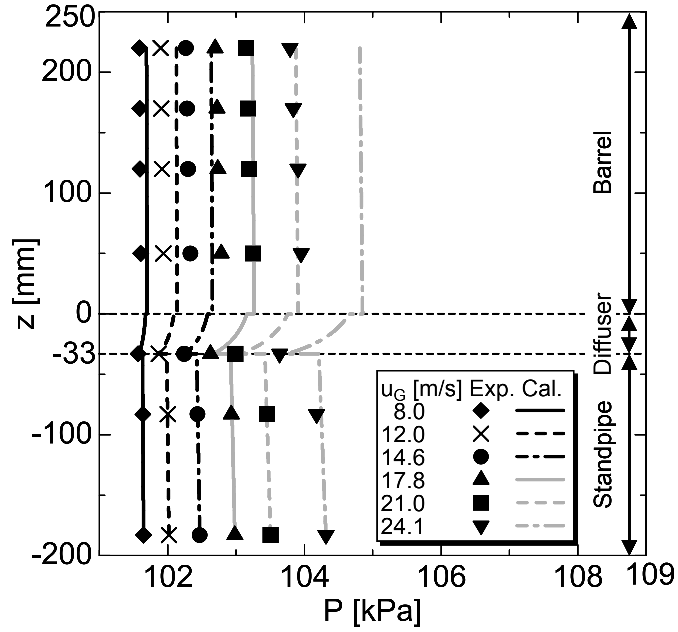

(a) Gas single-phase flow

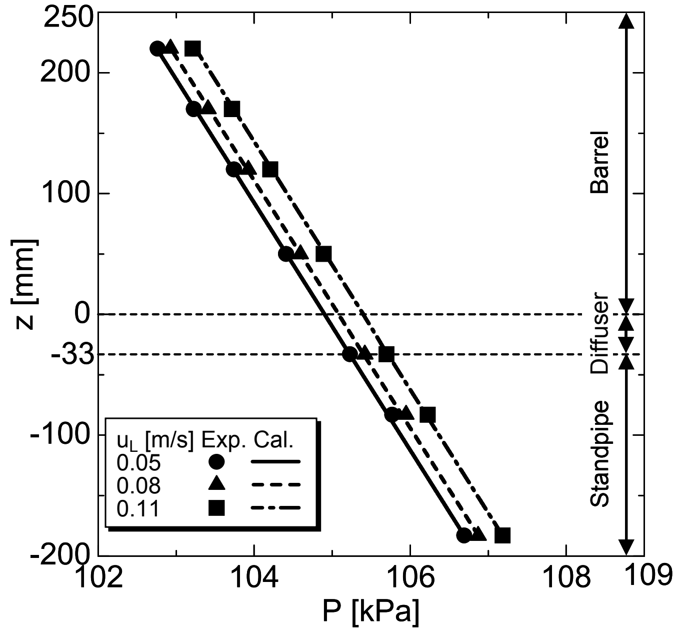

(b) Liquid single-phase flow

Fig. 7 Axial pressure distribution in swirling flow

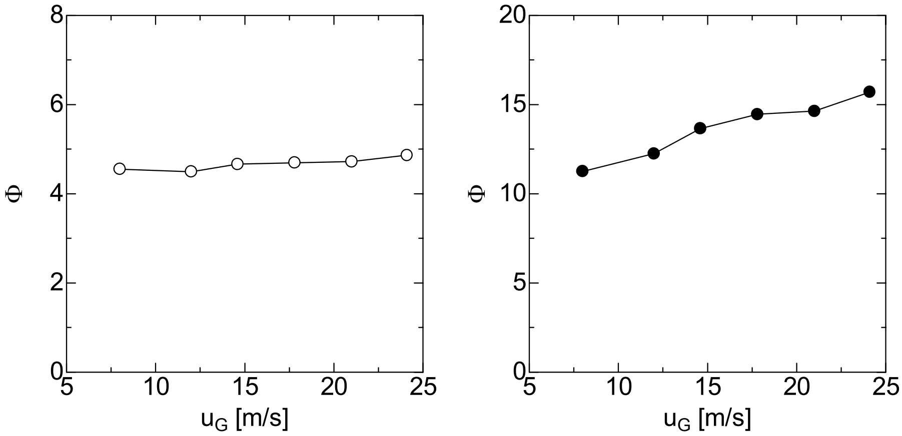

(a) Φ in the barrel (b) Φ in the diffuser

Fig. 8 Friction multiplier Φ for swirling flow

4. Results and Discussion

4.1. Pressure distribution in single-phase flow

Figure 6 shows comparisons between measured and predicted axial distributions of pressure in single-phase non-swirling flows. The 1D single-fluid model gives good predictions for the gas single-phase and liquid single-phase flows. It should be also noted that the pressure recovery in the diffuser is accurately predicted just by taking the diffuser geometry into account, and that the pressure drops in the barrel and standpipe are well evaluated by using the standard correlations, Eq.(4) and (5), for the friction factor.

Figure 7 shows comparisons for single-phase swirling flows. In the gas single-phase flows, the predicted pressure in the barrel is larger than the measured one. The pressure recovery in the diffuser is also overestimated. On the other hand, the pressure distributions in the liquid single-phase swirling flows are well predicted because the static pressure drop dominates the other contributions to the total pressure drop.

Nissan et al. [(10)] pointed out that the friction factor f_w in a swirling pipe flow is several times as large as that in a non-swirling flow. A multiplier Φ was, therefore, applied to f_w. An optimum value of Φ at each flow condition was determined as the value which made the following error Er less than 1 %.

$$Er = \left| 1 - \frac{(dP/dz)_{\mathrm{cal}}}{(dP/dz)_{\mathrm{exp}}} \right| \qquad (19)$$

Figure 8 (a) and (b) show the optimum values of Φ in the barrel and diffuser, respectively. The former ranges from 4.5 to 5.0 and slightly increases with u_G, whereas the latter clearly increases with u_G. Hence, the calculation was conducted using a constant value of Φ (= 4.6) for the barrel and the optimum values for the diffuser.

Comparisons are shown in **Fig. 9**. Good agreements are obtained by using the constant multiplier Φ in the barrel.

4.2. Pressure gradient and liquid film thickness in annular swirling flow

We also applied the friction multiplier Φ to the friction terms in the 1D two-fluid model to account for the effects of swirling flow on the interfacial and wall frictions. As is well known, the interfacial shear stress in an annular flow satisfies [(11)]

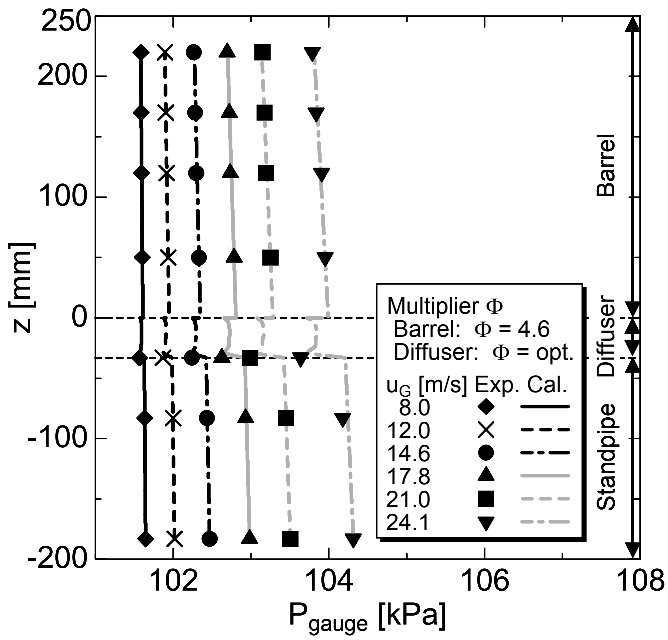

Fig. 9 Predictions using the friction multiplier Φ

$$\tau_i = \tau_w + \rho_L g \delta_{mean} \tag{20}$$

The wall shear stress τ_w is much larger than $\rho_L g \delta_{mean}$, and therefore, the above equation implies that the increase in τ_w induced by swirling flow is to be directly reflected in the increase in τ_i. Hence the constant multiplier, $\Phi = 4.6$, was applied not only to the wall friction f_w but also to the interfacial friction f_i.

Figures 10 and 11 are comparisons between measured and predicted pressure gradients dP/dz and film thicknesses δ at z = 170 mm. The predicted dP/dz and δ are in good agreement with the measured data except at J_G = 24.1 m/s. The multiplier Φ should be slightly larger than 4.6 at large gas volume fluxes as shown in Fig. 8 (a). This is the reason why dP/dz is slightly underestimated and δ is overestimated at J_G = 24.1 m/s. The difference between the measured and predicted liquid film thicknesses also slightly increases with J_L. This difference must be due to the assumption of no droplet flow in the two-fluid simulation, i.e., the droplet flow rate in the experiments must have gradually increased with J_L, which made the measured film thickness smaller than the predictions based on the assumption of no droplets. At any rate, we could confirm that the film thickness and pressure gradient of a swirling annular flow are well predicted by introducing a constant friction multiplier to the two-fluid model.

Then, to examine a difference between the air-water system and the steam-water system, two-fluid simulations were carried out using fluid properties of the saturated steam-water system at 7MPa. **Figure 12** shows comparisons of pressure drop and liquid film thickness between the two systems. The pressure drops in the steam-water system is much larger than that in the air-water system. This is mainly due to the increase in the gas density ρ_G. The film thickness in the former is much smaller than that in the latter. This is due to the increase in the interfacial shear stress τ_i. Note that τ_i is proportional to the gas density ρ_G.

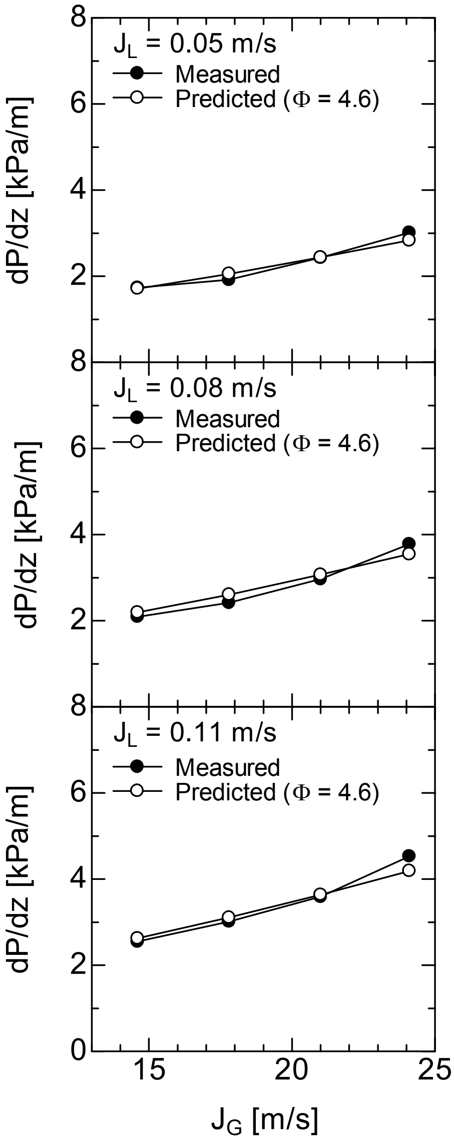

Fig. 10 Pressure gradient at z = 170 mm

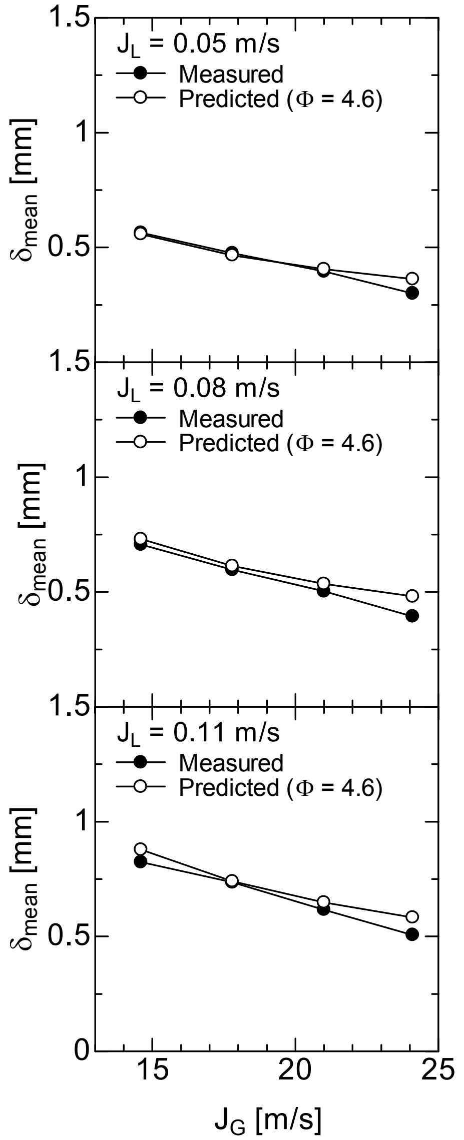

Fig. 11 Film thickness at z = 170 mm

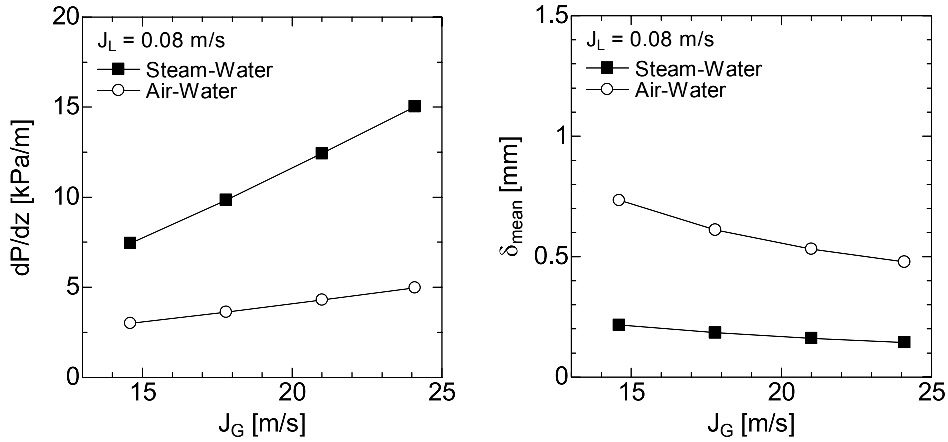

(a) Pressure gradient *dP/dz* (b) Liquid film thickness δ

Fig. 12 Pressure gradient and liquid film thickness in steam-water system

5. Conclusion

Pressure drops and liquid film thicknesses in swirling annular flows in the one-fifth scale model of the BWR steam separator were measured using differential pressure transducers and a laser focus displacement meter. Numerical simulations based on one-dimensional single-fluid and two-fluid models were also carried out to examine the feasibility of predicting pressure drop and film thickness in swirling flows. As a result, the following conclusions were obtained.

(1) The pressure drop in a single-phase swirling flow is several times as large as that in a non-swirling flow due to the increase in the frictional pressure drop.

(2) The pressure gradient and liquid film thickness in a two-phase swirling annular flow at the inlet of the first POR of the separator are accurately predicted by using a standard one-dimensional two-fluid model, provided that the interfacial and wall frictions in an ordinary two-phase annular flow are multiplied by appropriate constant values.

Acknowledgments

The authors gratefully acknowledge the financial support by "Innovation and Viable Nuclear Energy Technology Development Project", Ministry of Economy, Trade and Industry, Japan, and the assistance in experiments by Mr. D. Nishiwaki and Mr. T. Nariai.

References

(1) Nakao, T., Murase, M., Ishida, N., Kawamura, T., Minato, A. and Moriya, K., "Decreasing of Pressure Loss in BWR Steam Separator (1)", *Japanese J. of Multiphase Flow*, **Vol. 15**, No. 4, pp. 382-389. (2001).

(2) Terasaka, H. and Shimizu, S., "Two-Phase Flow Simulation around Swirler in a BWR Steam Separator", *Proceeding of 15th CFD Symposium.*, 1, pp. 1-5. (2001)

(3) Kataoka, H., Tomiyama, A., Hosokawa, S., Sou, A. and Chaki, M., "Two-Phase Swirling Flow in a Gas-Liquid Separator", *Journal of Power and Energy Systems*, **Vol. 2**, No. 4, pp.1120-1131. (2008).

(4) Kataoka, H., Tomiyama, A., Hosokawa, S., Sou, A. and Chaki, M., "Swirling Annular Flow in a Steam Separator", *Journal of Engineering for Gas Turbines and Power*, **Vol. 131**, Paper No. 032904, pp. 1-7. (2009).

(5) Kataoka, H., Tomiyama, A., Hosokawa, S., Sou, A. and Chaki, M., "Effects of Pick-Off-Ring Configuration on Separation Performance of a Gas-Liquid Separator", *Progress in Multiphase Flow Research*, **Vol. 3**, pp.67-74. (2008).

(6) Kataoka, H., Shinkai, Y. and Tomiyama, A., "Effects of Swirler Shape on Two-Phase Swirling Flow in a Steam Separator", *Journal of Power and Energy Systems*. (2009) to be published.

(7) Ikeda, H., Shimizu, T., Narabayashi, T., Kondo, T., Nishida, K. and Fukuda, "T., Improvement of BWR Steam Separator with Three-dimensional Gas-Liquid Two-Phase Flow Simulation Method", *on CD-ROM of 11th International Conference on Nuclear Engineering (ICONE-11)*, Paper No. 36486, pp. 1-9. (2003).

(8) Takamasa, T. and Hazuku, T., "Measuring a Film Flowing Down a Vertical Wall Using Laser Focus Displacement Meters (1st Report, Measuring Principle and Film Thickness.) ", *Transactions of The Japan Society of Mechanical Engineers*, Ser. B, **Vol. 64**, No. 617, pp.128-135. (1998), in Japanese.

(9) Wallis, G. B., *One Dimensional Two-Phase Flow*, McGraw-Hill, pp. 318-322. (1969).

(10) Nissan, A. H. and V. P. Bresan, "Swirling Flow in Cylinders", *The American Institute of Chemical Engineers Journal*, **Vol. 7**, No. 4, pp.543-547. (1961).

(11) G. F. Hewitt, and N. S. Hall-Taylor, *Annular Two-phase Flow*, Pergamon, pp.57-60. (1970).